



**HAL**  
open science

# Formation of CO, CH<sub>4</sub>, H<sub>2</sub>CO and CH<sub>3</sub>CHO through the H<sub>2</sub>CCO + H surface reaction under interstellar conditions

Mohamad Ibrahim, Jean-Claude Guillemin, Patrick Chaquin, Alexis Markovits, Lahouari Krim

► **To cite this version:**

Mohamad Ibrahim, Jean-Claude Guillemin, Patrick Chaquin, Alexis Markovits, Lahouari Krim. Formation of CO, CH<sub>4</sub>, H<sub>2</sub>CO and CH<sub>3</sub>CHO through the H<sub>2</sub>CCO + H surface reaction under interstellar conditions. *Physical Chemistry Chemical Physics*, 2022, 24 (38), pp.23245-23253. 10.1039/D2CP02980D . hal-04248817

**HAL Id: hal-04248817**

**<https://hal.science/hal-04248817>**

Submitted on 18 Oct 2023

**HAL** is a multi-disciplinary open access archive for the deposit and dissemination of scientific research documents, whether they are published or not. The documents may come from teaching and research institutions in France or abroad, or from public or private research centers.

L'archive ouverte pluridisciplinaire **HAL**, est destinée au dépôt et à la diffusion de documents scientifiques de niveau recherche, publiés ou non, émanant des établissements d'enseignement et de recherche français ou étrangers, des laboratoires publics ou privés.

# Formation of CO, CH<sub>4</sub>, H<sub>2</sub>CO and CH<sub>3</sub>CHO through the H<sub>2</sub>CCO + H surface reaction under interstellar conditions

Mohamad Ibrahim<sup>1</sup>, Jean-Claude Guillemin<sup>2</sup>, Patrick Chaquin<sup>3</sup>, Alexis Markovits<sup>3</sup> and Lahouari Krim<sup>1\*</sup>

<sup>1</sup>Sorbonne Université, CNRS, De la Molécule aux Nano-Objets: Réactivité, Interactions, Spectroscopies, MONARIS, 75005, Paris, France.

<sup>2</sup>Univ Rennes, Ecole Nationale Supérieure de Chimie de Rennes, CNRS, ISCR – UMR6226, F-35000 Rennes, France.

<sup>3</sup>Sorbonne Université, CNRS, Laboratoire de Chimie Théorique, LCT, 75005, Paris, France.

\*Corresponding author: Lahouari.krim@Sorbonne-universite.fr

## Abstract

The reaction of ketene (H<sub>2</sub>CCO) with hydrogen atoms has been studied under interstellar conditions through two different experimental methods, occurring on the surface and in the bulk of H<sub>2</sub>CCO ice. We show that ketene interacting with H-atoms at 10 K leads mainly to four reactions products, carbon monoxide (CO), methane (CH<sub>4</sub>), formaldehyde (H<sub>2</sub>CO) and acetaldehyde (CH<sub>3</sub>CHO). A part of these results shows a chemical link between a simple organic molecule such as H<sub>2</sub>CCO and a complex one such as CH<sub>3</sub>CHO, through H-addition reactions taking place in dense molecular clouds. The H-addition processes are very often proposed by astrophysical models as mechanisms for the formation of complex organic molecules based on the abundances of species already detected in the interstellar medium. However, the present study shows that the hydrogenation of ketene under non-energetic conditions may also lead efficiently to fragmentation processes and to the formation of small species such as CO, CH<sub>4</sub> and H<sub>2</sub>CO, without supplying external energy such as UV photons or high energy particles. Such fragmentation pathways should be included in the astrophysical modeling of H<sub>2</sub>CCO + H in molecular clouds of the interstellar medium. To support these results, theoretical calculations have explicitly showed that, under our experimental conditions, H-atom interactions with of C=C bound of ketene leads mainly to CH<sub>3</sub>CHO, CH<sub>4</sub> and CO. By investigating the formation and reactivity of the reaction intermediate H<sub>3</sub>C-C=O radical, our calculations demonstrate that H<sub>3</sub>C-C=O + H reaction evolves throughout two barrierless pathways to form either CH<sub>3</sub>CHO or CH<sub>4</sub> and CO fragments.

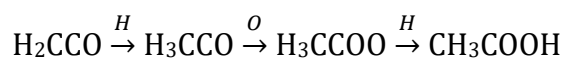
## 1. Introduction

More than 70 species detected in the Interstellar Medium (ISM) and containing at least six atoms of C, H, O, or N are called complex organic molecules (COMs).<sup>1</sup> These COMs have been detected in several astrophysical environments<sup>2-4</sup> such as pre-stellar cores and interstellar clouds. Although molecular hydrogen is the main component of the dark clouds, many organic compounds may form through surface reactions involving atoms such as H, O, C and N and simple chemical species and lead to more complex interstellar closed-shell molecules and radicals such as formyl, ketenyl, aldehydes, alcohols, and sugars. The spatial distributions and abundances of such COMs depend strongly on the extreme conditions of the ISM where their formation reactions take place. The simultaneous detection of many organic compounds toward the same astronomical environment has led to many theoretical and experimental investigations in order to find the chemical links between the detected species and to explain the interstellar formation of many COMs. In the recent years, a number of observational investigations, theoretical and experimental studies have been carried out focusing on the formation and transportations routes of ketene molecule.<sup>5-10</sup> Ketene was detected in space for the first time by Turner et al. 1977<sup>11</sup> in the dense molecular cloud Sagittarius B2. Then many astronomical observations have reported its detection in massive hot cores and giant molecular clouds such as Orion KL and TMC-1,<sup>12,13</sup> in the gas phase of translucent clouds (CB 17, CB 24, and CB 228),<sup>14</sup> toward the prestellar core L1689B, extragalactic source PKS 1830–211, and in several deeply embedded protostars (AFGL 989, WL 22, NGC 6334I, NGC 7538 I1).<sup>15-17</sup> However, the first simultaneous observation of HCCO, H<sub>2</sub>CCO and CH<sub>3</sub>CHO showing saturated and unsaturated species derived from ketene, has been performed by Agúndez et al 2015<sup>18</sup> toward the starless core Lupus-1A and the molecular cloud L483. Such a simultaneous detection would suggest that sequential H-addition reaction, the most likely reaction in molecular clouds, would turn HCCO in H<sub>2</sub>CCO and CH<sub>3</sub>CHO:



Despite the fact that the radical HCCO was found approximately ten and five times less abundant than H<sub>2</sub>CCO and CH<sub>3</sub>CHO, respectively, Agúndez et al 2015<sup>18</sup> did not observe radical species such as acetyl radical (H<sub>3</sub>CCO) or vinoxyl radical (H<sub>2</sub>CCHO) which are the

potential reaction intermediates during the hydrogenation of ketene ( $\text{H}_2\text{CCO}$ ) to form acetaldehyde ( $\text{H}_3\text{CCHO}$ ). The non-detection of these two radicals would suggest that they would be very instable and reactive and may involve in several reaction mechanisms such as the formation of  $\text{CH}_3\text{CHO}$  through successive hydrogenation of ketene or that of glycolaldehyde ( $\text{CHOCH}_2\text{OH}$ ) and acetic acid ( $\text{CH}_3\text{COOH}$ ) which involves O- and H- addition reactions.



These reaction mechanisms indicate the important role of ketene in the chemical complexification of the interstellar medium which starting from simple species such as ketene leads to three molecules playing an important role in prebiotic chemistry.<sup>19</sup> In this context, three isomers of  $\text{C}_2\text{O}_2\text{H}_4$  have been detected in the ISM; glycolaldehyde ( $\text{HCOCH}_2\text{OH}$ )<sup>20</sup>, methyl formate ( $\text{HCOOCH}_3$ )<sup>21</sup> and acetic acid ( $\text{CH}_3\text{COOH}$ )<sup>22</sup>. Noting that glycolaldehyde is the least abundant of three isomers. This would suggest that compared to acetic acid and methyl formate, glycolaldehyde could be very reactive and successive hydrogenations would turn it into ethylene glycol ( $\text{HOCH}_2\text{CH}_2\text{OH}$ ). This reaction pathway has been investigated experimentally by our group<sup>23</sup>, showing that  $\text{CHOCH}_2\text{OH} + 2\text{H}$  solid phase reaction leads to  $\text{HOCH}_2\text{CH}_2\text{OH}$ . In the present work, we have experimentally investigated the solid state hydrogenation of  $\text{H}_2\text{CCO}$  molecule under ISM conditions with the goal to validate or invalidate the formation of species such as  $\text{H}_3\text{CCO}$ ,  $\text{H}_2\text{CCHO}$  and  $\text{CH}_3\text{CHO}$ . In section 2, we describe our experimental setup and the calculation methods, and then we report in section 3 the experimental and theoretical results obtained for  $\text{H}_2\text{CCO} + \text{H}$  reaction. Discussions and conclusions about the results are presented in sections 4 and 5.

## 2. Experimental and calculation methods

The experimental setup used in this study has been described in detail previously.<sup>24</sup> The solid samples are formed by condensation of gas reactants. The formation of the solid sample is performed under ultrahigh vacuum at  $10^{-10}$  mbar through a condensation of the  $\text{H}_2\text{CCO}$  onto one of six flat, highly polished, rhodiated copper mirror maintained at 10 K using a pulsed tube closed-cycle cryogenerator (Sumitomo cryogenics F-70) and programmable temperature controller (Lakeshore 336). The metal mirror is positioned perpendicularly to the  $\text{H}/\text{H}_2$  beam derived from an atomic source. Atomic-H is produced by a microwave driven atom source (SPECS PCR-ECS). This source uses a microwave discharge to generate gas plasma in a chamber fed with molecular hydrogen.  $\text{H}$  gas is injected in the reaction chamber at a pressure of  $10^{-5}$  mbar with an  $\text{H}$ -atom flux calculated around  $1 \times 10^{15}$  atoms  $\text{cm}^{-2} \text{s}^{-1}$ . The gas leaving the chamber is a combination of both atomic and molecular hydrogen ( $\text{H}/\text{H}_2$ ) with a dissociation yield of 15%. Ketene produced by thermolysis of acetic anhydride at  $900^\circ\text{C}$  is selectively condensed and stored under vacuum in a reservoir at  $-196^\circ\text{C}$  in liquid nitrogen. To introduce ketene vapor into the injection ramp to form our solid samples, a cooling bath made of ethanol and liquid nitrogen maintained at  $-110^\circ\text{C}$  allows the frozen  $\text{H}_2\text{CCO}$  to partially evaporate. The pressure in the injection ramp is measured with a digital Pirani gauge, while the fractions of ketene gas injected into the experimental chamber are controlled using a leak valve. Infrared spectra were recorded in the transmission-reflection mode between 5000 and  $500 \text{ cm}^{-1}$ , with a resolution of  $0.5 \text{ cm}^{-1}$ , using a Bruker 120 FTIR spectrometer with an incidence<sup>25</sup> angle of  $8^\circ$ . The hydrogenation of ketene in solid state has been carried out through two different experiments:

- Exp 1,  $\text{H}_2\text{CCO} + \text{H}$  surface reaction: bombardment of ketene ice by  $\text{H}$ -atoms at 10 K.
- Exp 2,  $\text{H}_2\text{CCO} + \text{H}$  bulk reaction: co-injection of ketene and  $\text{H}$ -atoms at 10 K.

In Exp 1, ketene ices are formed at 10 K and subsequently bombarded by  $\text{H}$ -atoms during 45 min while in Exp 2,  $\text{H}$ -atoms are co-injected with pure ketene (during 30 min).

For the theoretical part, geometry optimizations and vibrational frequencies have been performed at the MP2/cc-pVTZ level, followed by a single point CCSD(T) energy calculation. Nevertheless, dealing the transition states TS1 and TS2 which are of critical

importance for the overall reaction scheme, additional geometry optimization and vibration frequencies have been done at the CCSD/cc-pvtz level. All results include zero-point (ZPE) correction. The GAUSSIAN 09 series of program has been used throughout the work.<sup>26</sup>

### 3. Results

Figures 1a and 1b show the IR spectra of ketene ice formed at 10 K, before and after H-bombardments, respectively.

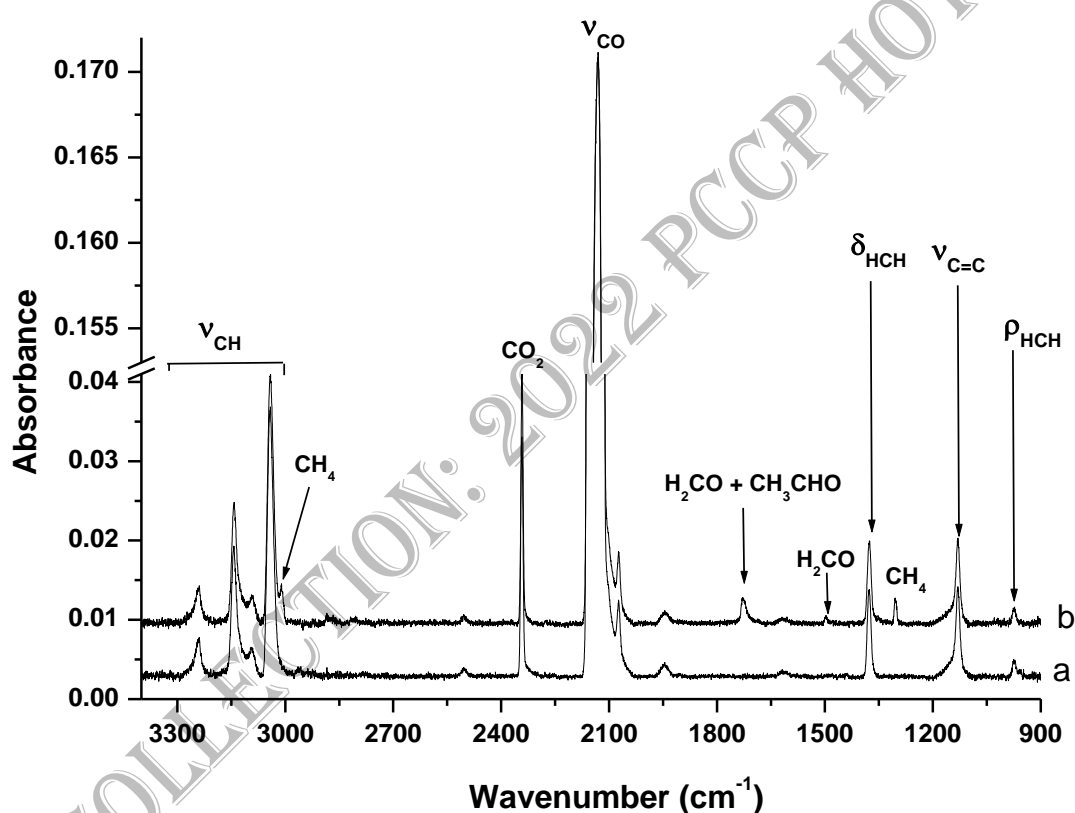


Figure 1: a) IR spectrum of ketene ice formed at 10 K. b) IR spectrum of ketene ice after H-bombardments. ( $\nu$ ,  $\rho$  and  $\delta$  refer to the stretching, rocking and bending modes, respectively)

The IR spectrum of solid H<sub>2</sub>CCO is characterized by a strong IR signal at 2114 cm<sup>-1</sup> corresponding to C=O stretching mode, two signals at 3143 and 3041 cm<sup>-1</sup> feature of C=H stretching modes, a band at 1129 cm<sup>-1</sup> corresponding to C=C stretching mode, and

two signals at 972 and 1376  $\text{cm}^{-1}$  attributed to  $\text{CH}_2$  rocking and bending modes, respectively. In addition to overtone and combination bands, the natural isotopomer of ketene  $\text{CH}_2^{13}\text{CO}$  shows an IR signal at 2073  $\text{cm}^{-1}$ , corresponding to  $^{13}\text{C}=\text{O}$  vibration. The bands attributions are provided in table 1.

Table1: Assignments of IR absorption bands of Ketene ice

Position (Ref) <sup>27</sup> ( $\text{cm}^{-1}$ )	Present work ( $\text{cm}^{-1}$ )	Assignments <sup>28</sup>
3043	3041	C-H str
2133	2114	C=O str
1374	1376	H-C-H bend
1131	1129	C=C str
3140	3143	C-H str
971	972	$\text{CH}_2$ rock
440-435	-	C=C=O bend
616	-	$\text{CH}_2$ wag
529, 512	515	C=C=O bend
1942	1945	Overtone band( $\text{CH}_2$ rock)
3234	3239	Combination band (C=O str+C=C str)
-	4230	Combination band (C-H str+C=C str)
2075	2073	C=O str ( $^{13}\text{C}$ )

We note from figure 1.b corresponding to the infrared spectrum of the  $\text{H}_2\text{CCO}$  ice after H-bombardments that new IR signals appear at 3012, 1728, 1500, 1351 and 1304  $\text{cm}^{-1}$  after hydrogenation processes and they may be assigned to the reaction products formed through  $\text{H}_2\text{CCO} + \text{H}$  surface reaction at 10 K. First, the two bands observed at 3012 and 1304  $\text{cm}^{-1}$  are easily attributed to  $\nu_3$  and  $\nu_4$  modes of  $\text{CH}_4$ .<sup>29,30</sup> In order to characterize the ketene consumed after H-bombardments and to better identify the other reaction products, Figure 2 exposes a spectral zoom between 1100 and 2400  $\text{cm}^{-1}$ . Figures 2a and 2b show the IR spectra of  $\text{H}_2\text{CCO}$  ice formed at 10 K, before and after H-

bombardments, respectively, while Figure 2c shows the difference spectrum before and after H-bombardments of ketene ice.

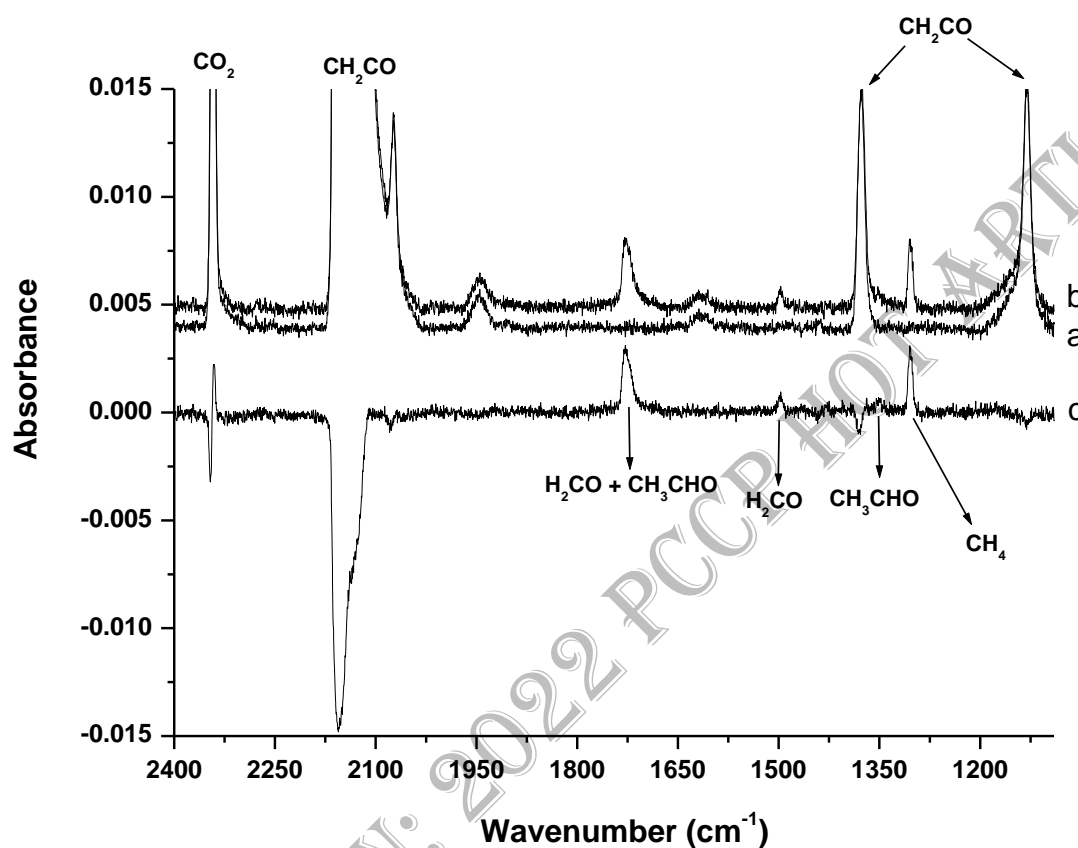


Figure 2: Zoom in 2400-1100  $\text{cm}^{-1}$  spectral region. IR spectrum of ketene ice formed at 10 K, a) before H-bombardment. b) After H-bombardment. c) Difference spectrum before and after H-bombardments of  $\text{H}_2\text{CCO}$ .

$\text{CO}_2$  (at  $2342 \text{ cm}^{-1}$ ) is an impurity in the  $\text{H}_2\text{CCO}$  sample and its IR signal remains constant during the hydrogenation process. The negative peak corresponding to the C=O stretching of  $\text{H}_2\text{CCO}$  in the difference spectrum of figure 2c indicate that almost 10 % of ketene is consumed to form new reaction products with positive IR signatures which may be assigned based on the previous solid phase studies. The observed signals at 1728 and  $1351 \text{ cm}^{-1}$  may be attributed to the C=O stretching and  $\text{CH}_3$  deformation modes of the acetaldehyde ( $\text{CH}_3\text{CHO}$ ). Previous experimental studies of interstellar ice analogs have already shown that  $\text{CH}_3\text{CHO}$  has two characteristic IR signals around 1728 and  $1351 \text{ cm}^{-1}$ .<sup>31-34</sup> However, the most intense IR signal observed at  $1728 \text{ cm}^{-1}$  and

assigned to C=O stretching mode of CH<sub>3</sub>CHO may also hide the  $\nu_{C=O}$  of formaldehyde (H<sub>2</sub>CO) as we also detect the most characteristic signal<sup>35,36</sup> of H<sub>2</sub>CO at 1500 cm<sup>-1</sup>. Previous studies<sup>37,38</sup> have shown that H<sub>2</sub>CO ice is characterized by two IR signals at 1723 and 1500 cm<sup>-1</sup> and corresponding to C=O stretching and CH<sub>2</sub> bending modes, respectively. Table 2 summarizes the new IR signals observed after H<sub>2</sub>CCO ice hydrogenation and their assignments based to the literature data.

Table 2: IR signals of the main products resulting from the hydrogenation of H<sub>2</sub>CCO ice.

Bands positions cm <sup>-1</sup>	Assignments	Ref
1304	CH <sub>4</sub>	30
1351	CH <sub>3</sub> CHO	31
1500	H <sub>2</sub> CO	35, 36
1728	CH <sub>3</sub> CHO + H <sub>2</sub> CO	32, 37, 38
3012	CH <sub>4</sub>	30

Based on this first experiment of bombardment of ketene ice by H-atoms at 10 K we may conclude that the H<sub>2</sub>CCO + H surface reaction leads mainly to CH<sub>4</sub>, H<sub>2</sub>CO and CH<sub>3</sub>CHO as reaction products formed in solid phase. CH<sub>4</sub> and H<sub>2</sub>CO would derive from fragmentation processes while CH<sub>3</sub>CHO would result from H addition reaction on C=C of H<sub>2</sub>CCO. However, the H-addition reaction may also occur on the oxygen atom of C=O bound to form vinyl alcohol H<sub>2</sub>C=CHOH. In fact, from figures 1b, 2b and 2c, we notice that no efficient formation CH<sub>2</sub>CHOH occurs under our experimental conditions, since no absorption signal is detected around 1639 cm<sup>-1</sup> which is the most characteristic of the C=C stretching mode of vinyl alcohol. After the IR characterization of H<sub>2</sub>CCO + H surface reaction at 10 K, our interest has been focused on how to amplify the amount of the reaction products by increasing the probability of interactions between H-atoms and H<sub>2</sub>CCO. In fact, during the H-bombardment of ketene ice, all the processes occur on the first layer of H<sub>2</sub>CCO ice which may limit the reaction yield. Consequently, we have carried out Exp 2 of H<sub>2</sub>CCO/H/H<sub>2</sub> co-injection at 10K, where H<sub>2</sub>CCO, H and H<sub>2</sub> are co-deposited simultaneously during 30 min. Figure 3b shows the IR spectrum resulting from the H<sub>2</sub>CCO/H/H<sub>2</sub> co-injection at 10 K in the 2100-900 cm<sup>-1</sup> spectral region. As a reference spectrum, figure 3a shows the IR spectrum corresponding to the H<sub>2</sub>CCO/H<sub>2</sub> co-injection.

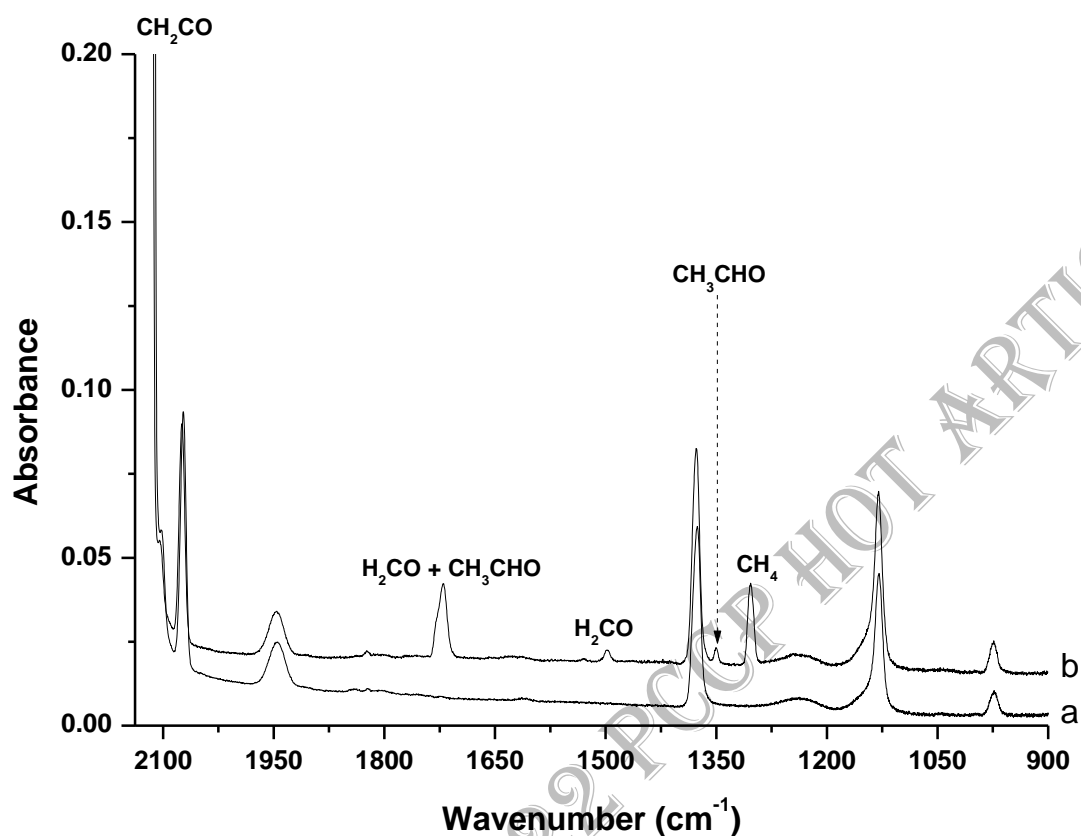


Figure 3: Co-injection experiment at 10 K. a)  $\text{H}_2\text{CCO} + \text{H}_2$  reaction. b)  $\text{H}_2\text{CCO} + \text{H} + \text{H}_2$  reaction.

Comparison of figures 3a, 3b shows that the  $\text{H}_2\text{CCO}/\text{H}/\text{H}_2$  co-injection experiment leads to the same reaction products obtained after H bombardments of the  $\text{H}_2\text{CCO}$  ice. Besides the absorption bands at 1728, 1500, 1351 and 1304  $\text{cm}^{-1}$ , no additional IR signals are detected during the co-injection experiment which only increases the amount of  $\text{CH}_4$ ,  $\text{H}_2\text{CO}$  and  $\text{CH}_3\text{CHO}$ , reaction products already detected during the first experiment EXP1. The IR Signals detected at 1500, 1351  $\text{cm}^{-1}$  are more visible in figure 3b in comparison with figure 2c, and this confirms our assignment to  $\text{H}_2\text{CO}$  and  $\text{CH}_3\text{CHO}$ , respectively. In order to estimate the amounts of the ketene consumed and those of  $\text{CH}_4$ ,  $\text{H}_2\text{CO}$  and  $\text{CH}_3\text{CHO}$  formed, column densities of the reactants and products have been calculated for the two experiments EXP1 and EXP2. The column densities  $n$  ( $\text{molec cm}^{-2}$ ) are directly deduced from the IR integrated intensities as:

$$n = \frac{\ln 10 \int I(\nu) \cos(8^\circ)}{\varepsilon \cdot 2}$$

$\int I(\nu)$  is the integrated peak area of the considered vibrational mode. The  $\cos(8^\circ)/2$  is a correction term which take into account the geometry of our IR measurements.<sup>39</sup> Table 3 shows the vibrational modes considered for our calculations and their corresponding band strengths.

Table 3: Vibrational modes, spectral positions and band strengths of H<sub>2</sub>CCO, CH<sub>4</sub>, H<sub>2</sub>CO and CH<sub>3</sub>CHO.

Molecule	Mode	Position band (cm <sup>-1</sup> )	$\varepsilon$ (cm molec <sup>-1</sup> )	reference
H <sub>2</sub> CCO	CH <sub>2</sub> bend.	1376	2.7 X 10 <sup>-18</sup>	40
	C=O stretch.	2114	1.2 X 10 <sup>-16</sup>	
CH <sub>4</sub>	CH <sub>2</sub> bend	1304	8.0 x 10 <sup>-18</sup>	41
	C-H stretch.	3012	1.1 x10 <sup>-17</sup>	
H <sub>2</sub> CO	CH <sub>2</sub> bend.	1500	5.1 x 10 <sup>-18</sup>	41
	C=O stretch.	1723	1.6 x 10 <sup>-17</sup>	
CH <sub>3</sub> CHO	CH <sub>2</sub> bend.	1351	4.5 x 10 <sup>-18</sup>	32
	C=O stretch.	1728	3 x 10 <sup>-17</sup>	

Table 4 shows the amounts of the reactant consumed and products formed for H<sub>2</sub>CCO + H surface reaction from EXP 1, compared to the column densities obtained for the H<sub>2</sub>CCO + H co-injection experiments from EXP 2.

Table 4: Column densities (molec cm<sup>-2</sup>) of reaction products formed during H<sub>2</sub>CCO + H solid state reactions from EXP1 and EXP2.

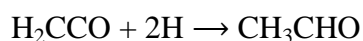
	H <sub>2</sub> CCO	CH <sub>4</sub>	H <sub>2</sub> CO	CH <sub>3</sub> CHO
EXP1				
H <sub>2</sub> CCO ice at 10 K before H-bombardment	6.0 10 <sup>16</sup>	0	0	0
H <sub>2</sub> CCO ice at 10 K after H-bombardment	5.5 10 <sup>16</sup>	2.3 10 <sup>15</sup>	1.8 10 <sup>15</sup>	1.6 10 <sup>15</sup>
EXP2				
H <sub>2</sub> CCO + H Co-injection experiment at 10 K	3.5 10 <sup>17</sup>	3.6 10 <sup>16</sup>	0.9 10 <sup>16</sup>	0.8 10 <sup>16</sup>

From H<sub>2</sub>CCO + H surface reaction from EXP 1, we estimate that just after the H<sub>2</sub>CCO ice deposition at 10 K, the amount of ketene is 6.0×10<sup>16</sup> molec cm<sup>-2</sup> and just 5.0 ×10<sup>15</sup> molec cm<sup>-2</sup> are consumed after the H-bombardment showing that only 8 % of ketene is involved in the H<sub>2</sub>CCO + H surface reaction occurring at 10 K. As mentioned above, the H-bombardment of

ketene ice depends strongly on how the H-atoms penetrate into the bulk of the ice, a process which would occur only on the first layers of H<sub>2</sub>CCO ice which may limit the reaction yield. From these results we notice that we form almost the same amounts of the reaction products CH<sub>4</sub>, H<sub>2</sub>CO and CH<sub>3</sub>CHO around 2.0×10<sup>15</sup> molec cm<sup>-2</sup>. For H<sub>2</sub>CCO + H co-injection experiments from EXP 2, the amount of ketene consumed cannot be estimated. However, we notice that by increasing the probability of interactions between H-atoms and H<sub>2</sub>CCO and also the amount of H<sub>2</sub>CCO during the co-injection reaction, more reactions products are formed but with different distributions. While the same amounts of H<sub>2</sub>CO and CH<sub>3</sub>CHO are produced, the concentration of CH<sub>4</sub> is estimated to be almost four times higher than that of CH<sub>3</sub>CHO.

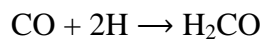
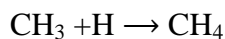
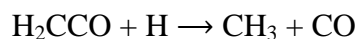
#### 4. Discussion

By investigating the H<sub>2</sub>CCO + H solid state reaction through two different experimental methods, reactions occurring on the H<sub>2</sub>CCO ice surface and those taking place in the bulk of the H<sub>2</sub>CCO ice, we show that ketene interacting with hydrogen atoms under interstellar conditions leads mainly to three reaction products CH<sub>4</sub>, H<sub>2</sub>CO and CH<sub>3</sub>CHO. We note that all these molecules are commonly detected in molecular clouds and then they can be linked by sequential dust grain surface reactions involving H atoms.<sup>42</sup> The first possible pathway for the H<sub>2</sub>CCO + H occurring on the ice surface or in the bulk of the ice would be a successive hydrogenation to convert H<sub>2</sub>CCO **1** into CH<sub>3</sub>CHO **4** (Channel 1). The H atoms attack the one of two C atoms of H<sub>2</sub>CCO to form CH<sub>3</sub>CO **2** or/and CH<sub>2</sub>CHO **3** radicals. Then, these two radicals would react with an additional hydrogen atom to form acetaldehyde (CH<sub>3</sub>CHO). However, the two reaction intermediates (CH<sub>3</sub>CO **2** and CH<sub>2</sub>CHO **3**) have not been detected in our IR spectra due probably to their high reactivity with H atoms.



The second pathway of the H<sub>2</sub>CCO + H solid state reaction is related to the C=C bond cleavage leading to CH<sub>3</sub> and CO for which IR signatures have not been detected in our IR spectra. CH<sub>3</sub> is a radical species showing high reactivity with H-atoms to form CH<sub>4</sub> through CH<sub>3</sub> + H radical-radical recombination. While the IR signal of CO which is located around 2138 cm<sup>-1</sup> would be hidden by the wide absorption band of the C=O stretching mode of H<sub>2</sub>CCO located at 2114 cm<sup>-1</sup>. CH<sub>3</sub> and CO, resulting from the fragmentation of H<sub>2</sub>CCO + H

system, can be then considered as the two reaction intermediates for formation of CH<sub>4</sub> and H<sub>2</sub>CO, the two reaction products under our experimental conditions.



In order to support the reaction pathways proposed, based on our experimental results, theoretical investigation have been carried out to determine the kinetic and thermodynamical parameters of the various reaction paths resulting from H addition to an isolated ketene molecule. Indeed, the gas phase reactions may differ significantly from the actual processes occurring with ice, but they provide a comparison of the competing paths and offer credible assumptions about the most probable mechanisms. The overall reaction scheme is displayed in Figure 4, focusing on the H-atom attack of C=C bound.

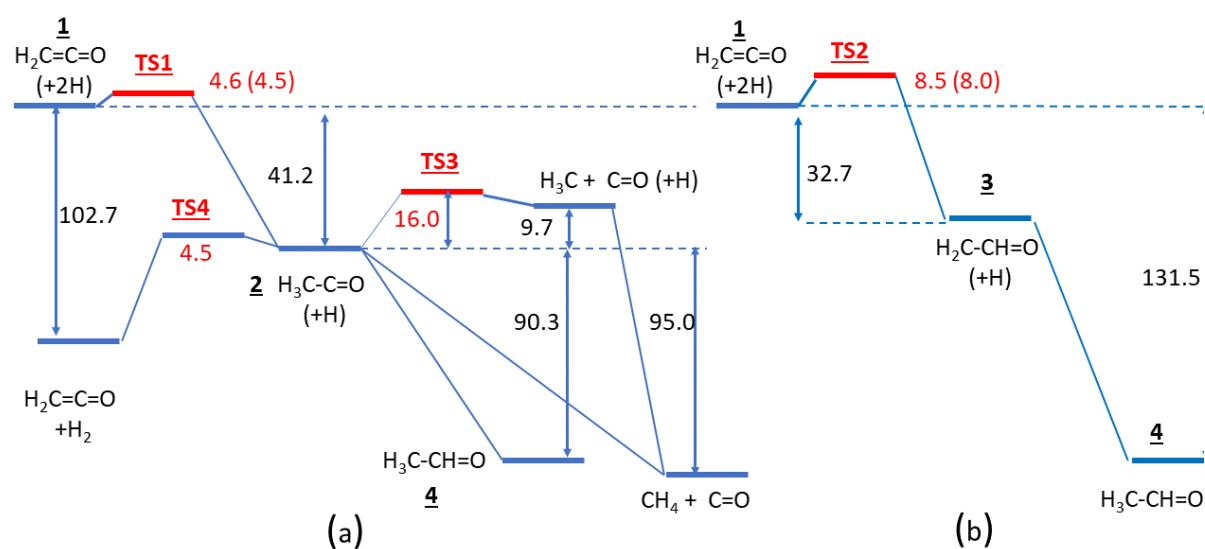


Figure 4: Reactions of ketene with atomic hydrogen: (a) H attack on terminal carbon; (b) H attack on central carbon; energies in kcal/mol; MP2/cc-pvtz level (CCSD/cc-pvtz).

The reaction of atomic hydrogen H on each carbon sites of ketene **1** yields radical H<sub>3</sub>C-C=O **2** with a 4.6 kcal activation energy (4.5 kcal/mol with CCSD level optimization), and radical H<sub>2</sub>C-CH=O **3** with an activation energy of 8.5 kcal/mol (8.0 kcal/mol with CCSD level optimization). The structures of radicals **2** and **3** and those of the transition states involved are shown in Figure 5. This suggests that ketene should yield much more efficiently H<sub>3</sub>CCO **2** than H<sub>3</sub>C-CH=O **3** under non-energetic conditions, though the crossing of the corresponding

energy barrier involves tunneling effects. By interacting with another H-atom,  $\text{H}_3\text{C-C=O}$  **2** evolves into two barrierless reaction pathways. It could be converted either into acetaldehyde **4** through radical-radical recombination or fragmented into  $\text{CH}_4 + \text{CO}$ .

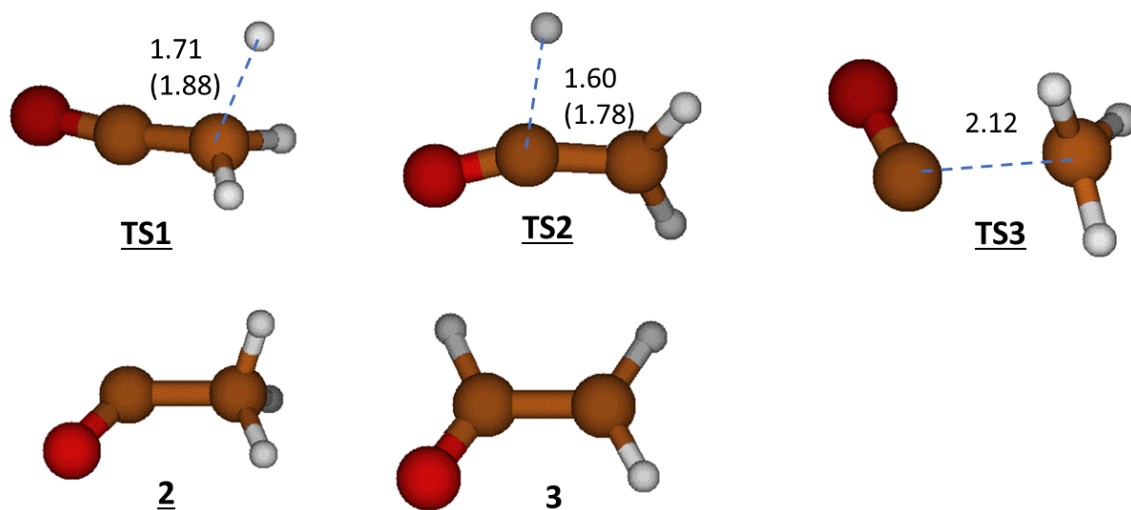


Figure 5: Structures of transition states and radicals **2** and **3**; distances in Å, MP2/cc-pvtz (CCSD/cc-pvtz).

The radical **3** is found less stable than **2** by 8.5 kcal/mol, though it is conjugated with C=O. But the unpaired electron in **3** is pure p whereas in **2** it is mainly located in a s+p MO, further stabilized by the electronegativity of oxygen (see Figure 6).

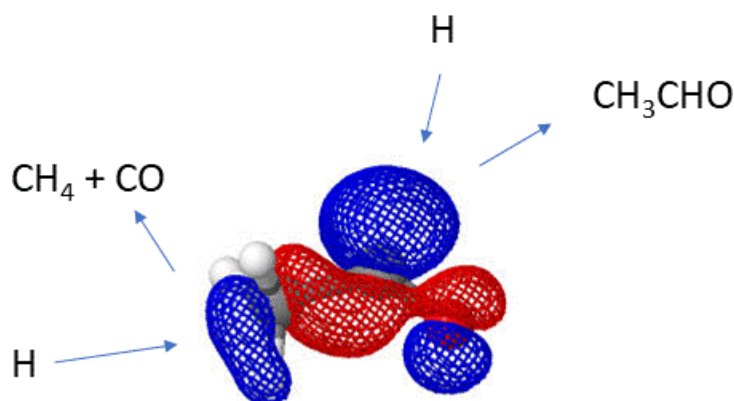


Figure 6: SOMO structure of radical **2** and scheme of its likely reactivity.

Both radicals 2 and 3 react on H without energy barrier to give acetaldehyde 4. However as mentioned above although both radicals 2 and 3 lead to acetaldehyde 4, only  $\text{H}_3\text{C}-\text{C}=\text{O}$  2 would be formed under our experimental conditions where  $\text{H}_2\text{CCO} + 2\text{H} \rightarrow \text{CH}_3\text{CHO}$  reaction occurs without supplying external energy such as UV photon or high energy particles, though the crossing of such an energy barrier involves tunneling effects. Two mechanisms are *a priori* possible to yield  $\text{CH}_4 + \text{CO}$  from 2. First, radical 2 may undergo a dissociation into  $\text{CH}_3 + \text{CO}$  which lies only 9.7 kcal/mol above but this path requires an activation energy of 16 kcal/mol (TS3) and thus should not be considered. Second (figure 7), the radical 2 reacts on atomic H getting close to  $\text{CH}_3$  in its “umbrella” region (see Figure 6); the system evolves without energy barrier towards  $\text{CH}_4 + \text{CO}$ :

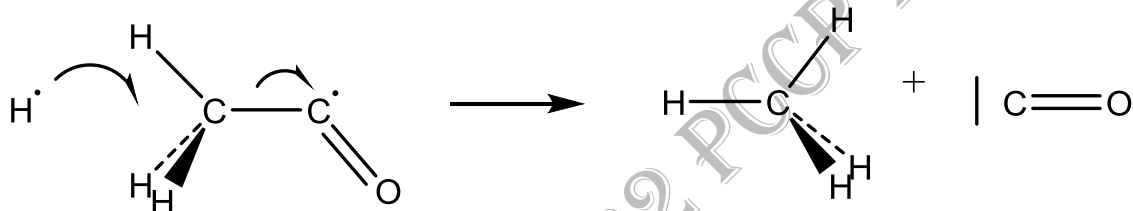
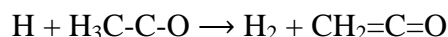


Figure 7: Reaction mechanism to yield  $\text{CH}_4 + \text{CO}$  from  $\text{H}_3\text{C}-\text{C}=\text{O}$  2 + H.

As a matter of fact, any attempt to characterize a transition state using the GAUSSIAN algorithms with various calculation methods (MP2, CCSD, B3LYP) has failed. The absence of energy barriers has been confirmed as follows. Considering that in the TSs involving a C-H bond, the carbon-hydrogen distance is always greater than 2 Å (cf. Figure 5), a hydrogen atom was put at this distance of the  $\text{CH}_3$  carbon, all other geometrical parameters frozen. The energy of this system lies slightly above (0.5 kcal/mol) that of the H plus  $\text{CH}_3-\text{CO}$  sum of energies. If now geometry optimization is allowed, the system evolves monotonously towards  $\text{CH}_4 + \text{CO}$ . Thus if an energy barrier is present, it is situated at  $\text{C}\dots\text{H} > 2 \text{ \AA}$  and should be very weak. This result, quite unexpected, is due to the strong exothermicity of the process (-90.3 kcal/mol), mainly arising from the high stability of CO. It is consistent with the weakness of the CC bond in 2, with only 9.7 kcal dissociation energy. It should be noted that the C=C bond in ketene itself is unusually weak, with a dissociation energy into  $\text{CH}_2 + \text{CO}$  of only 78.7 kcal/mol, less than that of a standard C-C single bond (90 kcal/mol for ethane).<sup>43</sup>

A third reaction of H with H<sub>3</sub>C-CO could *a priori* compete with the preceding ones, according to:



It involves the crossing of a barrier of 4.6 kcal/mol through **TS4** (see Figure 5), and thus is unlikely with respect to CH<sub>4</sub> + CO or CH<sub>3</sub>CHO formations.

The reactivity of radical **2** is well understood from the structure of its SOMO (Figure 6), which can lead either to acetaldehyde **4** or to CH<sub>4</sub> + CO according to the H approach. Consequently, the same amount of CO and CH<sub>4</sub> would derive from H<sub>2</sub>CCO + H solid state reaction. Under H attacks, CH<sub>4</sub> is not reactive, however part of the resulting CO may be converted into H<sub>2</sub>CO through the CO + 2H solid state reaction<sup>44,25</sup>. While the other part of CO remains trapped in the H<sub>2</sub>CCO ice, it cannot be observed directly in our IR spectra as its IR signal is hidden by the wide absorption band of H<sub>2</sub>CCO located at 2114 cm<sup>-1</sup>. Consequently, under our experimental conditions the [CH<sub>4</sub>] and [CO + H<sub>2</sub>CO] concentrations should be the same and the comparison between [CH<sub>4</sub>] and [CH<sub>3</sub>CHO] allows to estimate the branching ratios of the two channels involved into H<sub>2</sub>CCO + 2H reaction:

**EXPI:** [CH<sub>4</sub>] ~ [CH<sub>3</sub>CHO] ~ 2.0 10<sup>15</sup> molec cm<sup>-2</sup>, consequently, the two channels are equiprobable.



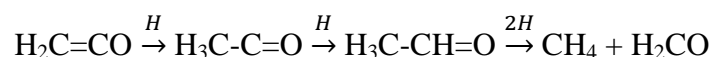
**EXP2:** [CH<sub>4</sub>] ~ 4.0 10<sup>16</sup> molec cm<sup>-2</sup> and [CH<sub>3</sub>CHO] ~ 1.0 10<sup>16</sup> molec cm<sup>-2</sup>, consequently, the channel leading to the molecular fragmentation is four times more efficient.



From the energy diagram of figure 4, we notice that once H<sub>3</sub>C-C=O **2** radical is formed, two competing reaction pathways appear for the barrierless process H<sub>3</sub>C-C=O + H and lead either to CH<sub>3</sub>CHO **4** or CH<sub>4</sub> + CO fragments. Our experimental results show that the formation of CH<sub>4</sub> and CO is favored for reactions taking place in the bulk of the H<sub>2</sub>CCO ice while, the two reaction pathways are equiprobable for processes occurring on H<sub>2</sub>CCO ice surface. The

efficient formation of CH<sub>4</sub> + CO as final reaction products can be directly linked to the two reactive sites of H<sub>3</sub>C-C=O **2** radical, during the H approach. As presented in figure 6, from the SOMO structure of radical **2**, the formation of CH<sub>3</sub>CHO **4** is due to the H-attack taking place on a limited space coplanar structure, a process which seems less likely than that occurring on C(sp<sup>3</sup>) with a tetrahedral structure and leading to CH<sub>4</sub> and CO fragments.

Another mechanism involving 4 hydrogen atoms and leading to CH<sub>4</sub> + H<sub>2</sub>CO could be considered.



However such a mechanism is less probable. We show in the present study that we form preferentially H<sub>3</sub>C-C=O as a first reaction intermediate through H<sub>2</sub>C=CO + H reaction. By interaction with another H atom, H<sub>3</sub>C-C=O evolves into two barrierless reaction pathways to be converted either into CH<sub>3</sub>CH=O or CH<sub>4</sub> + CO. To consider the formation of H<sub>2</sub>CO by the interactions with 4 hydrogen, the secondary reaction CH<sub>3</sub>-CH=O + 2H should take place and would also lead to ethanol. However we did not detect ethanol. In fact, methanol and ethanol are not detected under our experimental conditions and this is probably due to the small amounts of H<sub>2</sub>CO and CH<sub>3</sub>CHO formed during the hydrogenation process, compared to the huge concentration of the main reactant H<sub>2</sub>CCO. There is then a competition between the main reaction H<sub>2</sub>CCO + 2H which leads to CH<sub>3</sub>CHO, CO and CH<sub>4</sub> and the two secondary reactions H<sub>2</sub>CO + 2H and CH<sub>3</sub>CHO + 2H which involve reaction products.

## Conclusions

Four reaction products, carbon monoxide (CO), methane (CH<sub>4</sub>), formaldehyde (H<sub>2</sub>CO) and acetaldehyde (CH<sub>3</sub>CHO) have been characterized during the hydrogenation of ketene ice (H<sub>2</sub>CCO) at 10 K. Theoretical calculations have unambiguously showed that, under non energetic conditions, the reaction of atomic hydrogen H on carbon sites of ketene yields efficiently H<sub>3</sub>C-C=O which shows the lowest energy barrier during the H-addition reaction. Interacting with another H-atom, H<sub>3</sub>C-C=O leads to acetaldehyde as one on main reaction products. The detection of such a product shows a link between H<sub>2</sub>CCO and CH<sub>3</sub>CHO under interstellar conditions. Surprisingly, the H<sub>3</sub>C-C=O + H solid state reaction occurring at 10 K leads also to fragmentation processes without supplying external energy to yield CH<sub>4</sub> + CO.

CH<sub>4</sub> is not reactive and is detected as a final reaction product while a part of the resulting CO is converted into H<sub>2</sub>CO through the CO + 2H solid state reaction. This fragmentation pathway of ketene which should be included in astrophysical models, has been attributed to the reactivity of H<sub>3</sub>C-C=O radical and to the strong exothermicity of the reaction H<sub>3</sub>C-C=O + H → CH<sub>4</sub> + CO.

THEMED COLLECTION: 2022 PCCP HOT ARTICLES

## References

1. P. M. Woods, B. Slater, Z. Raza, S. Viti, W. A. Brown, and D. J. Burke, *Astrophys. J.*, 2013, **777** (2), 90
2. E. Herbst and E. F. van Dishoeck, *Annu. Rev. Astron. Astrophys.*, 2009, **47**, 427-480
3. T. Soma, N. Sakai, Y. Watanabe, and S. Yamamoto, *Astrophys. J.*, 2018, **854**, 116-127
4. A. Bacmann, A. Faure, and J. Berteaud, *ACS Earth Space Chem.*, 2019, **3**, 1000–1013
5. R. L. Hudson, M. J. Loeffler, *The Astrophysical Journal*, 2013, **773** : 109 (10pp)
6. S. Maity, R.I. Kaiser, and B. M. Jones, *ApJ*, 2014, **789**:36 (13pp)
7. A. M. Turner, A. S. Koutsogiannis, N. F. Kleimeier, A. Bergantini, C. Zhu, R. C. Fortenberry, and R. I. Kaiser, *ApJ*, 2020, **896**:88 (9pp)
8. K. Chuang, G. Fedoseev, D. Qasim, S. Ioppolo, C. Jager, Th. Henning, M. E. Palumbo, E. Van Dishoeck, and H. Linnartz, *A&A*, 2020, **635**, A199
9. K. Chuang, G. Fedoseev, C. Scirè, G.A. Baratta, C. Jager, Th. Henning, M. E. Palumbo, *A&A*, 2021, **650**, A85
10. G. Fedoseev, D. Qasim, K. Chuang, S. Ioppolo, T. Lamberts, E. Van Dishoeck, and H. Linnartz, *ApJ.*, 2022, **924**:110 (8pp)
11. Turner, B., *ApJL*, 1977, **213**, L75-79
12. L. Johansson, C. Andersson, J. Ellder, P. Friberg, A. Hjalmarsen, B. Hoglund, W. M. Irvine, H. Olofsson, G. Rydbeck, *A&A*, 1984, **130**, 227-256.
13. H. Matthews, and T. Sears, *ApJ*, 1986, **300**, 766
14. B. Turner, R. Terzieva, and E. Herbst, *ApJ*, 1999, **518**, 699-732
15. A. Bacmann, V. Taquet, A. Faure, C. Kahane, and C. Ceccarelli, *A&A*, 2012, **541**, L12
16. S. Muller, A. Beelen, M. Guélin, et al., *A&A*, 2011, **535**, A103
17. R. Ruiterkamp, S. B. Charnley, H. M. Butner, et al., *Astro. and Space Science*, 2007, **310**, 181-188
18. M. Agúndez, J. Cernicharo, and M. Guélin, *A&A*, 2015, **577**, L5
19. C.F. Chyba and K.P. Hand, *Annu. Rev. Astron. Astrophys.*, 2005, **43**, 31-74
20. J. M. Hollis, F. J. Lovas, P. R. Jewell, *ApJ*, 2000, **540**, L107
21. R. D. Brown, J. G. Crofts, F. F. Gardner, P. D. Godfrey, B. J. Robinson, J. B. Whiteoak, *ApJ*, 1975, **197**, L29
22. D. M. Mehringer, L. E. Snyder, Y. Miao, F. J. Lovas, *ApJ*, 1997, **480**, L71
23. K. Leroux, J. C. Guillemin, and L. Krim, *MNRAS*, 2021, **507**, 2632-2642
24. M. Jonusas, and L. Krim, *MNRAS*, 2017, **470**, 4564-4572
25. C. Pirim and L. Krim, *PCCP*, 2011, **13**, 19454–19459
26. Gaussian 09, Revision A.01, M. J. Frisch, G. W. Trucks, H. B. Schlegel, G. E. Scuseria, M. A. Robb, J. R. Cheeseman, G. Scalmani, V. Barone, B. Mennucci, G. A. Petersson, H. Nakatsuji, M. Caricato, X. Li, H. P. Hratchian, A. F. Izmaylov, J. Bloino, G. Zheng, J. L. Sonnenberg, M. Hada, M. Ehara, K. Toyota, R. Fukuda, J. Hasegawa, M. Ishida, T. Nakajima, Y. Honda, O. Kitao, H. Nakai, T. Vreven, J. A. Montgomery, Jr., J. E. Peralta, F. Ogliaro, M. Bearpark, J. J. Heyd, E. Brothers, K. N.

- Kudin, V. N. Staroverov, R. Kobayashi, J. Normand, K. Raghavachari, A. Rendell, J. C. Burant, S. S. Iyengar, J. Tomasi, M. Cossi, N. Rega, J. M. Millam, M. Klene, J. E. Knox, J. B. Cross, V. Bakken, C. Adamo, J. Jaramillo, R. Gomperts, R. E. Stratmann, O. Yazyev, A. J. Austin, R. Cammi, C. Pomelli, J. W. Ochterski, R. L. Martin, K. Morokuma, V. G. Zakrzewski, G. A. Voth, P. Salvador, J. J. Dannenberg, S. Dapprich, A. D. Daniels, Ö. Farkas, J. B. Foresman, J. V. Ortiz, J. Cioslowski, D. J. Fox, Gaussian, Inc., Wallingford CT, **2009**
27. C. B. Moore, and G. C. Pimentel, JCP, 1963, **38**, 2816-2829
28. W. D. Allen, and H. F. Schaefer, JCP, 1986, **84**, 2212-2225
29. O. Galvez, B. Mate, V. J. Herrero, and R. Escribano, ApJ, 2009, **703**, 2101–2107,
30. R. I. Kaiser, and , K. Roessler, ApJ, 1998, **503**, 959-975
31. M. H. Moore, and R. L. Hudson, Icarus, 1998, **135**, 518-527
32. C. J. Bennett, C. S. Jamieson, Y. Osamura, and R. I. Kaiser, 2005, ApJ, **624**, 1097 – 1115
33. S. E. Bisschop, W. G. Fuchs, E. F. van Dishoeck, and H. Linnartz, , A&A, 2007, **474**, 1061–1071
34. R. L. Hudson, and R. F. Ferrante, MNRAS, 2020, **492**, 283–293
35. B. Nelander, J. Chem. Phys, 1980, **73**, 1026-1033
36. W. A. Schutte, L. J. Allamandola, and , S. A. Sandford, Icarus, 1993, **104**, 118-137.
37. S. Maity , R. I. Kaiser, B. M. Jones, PCCP, 2015, **17**, 3081-3114
38. R. I. Kaiser, S. Maity, and B. M. Jones, PCCP, 2014, **16**, 3399-3424
39. C. J. Bennett, C. S. Jamieson, A. M. Mebel, and R. I. Kaiser, PCCP, 2004, **6**, 735- 746
40. Berg, O., & Ewing, G. E. 1991, JPhCh, 95, 2908
41. M. Bouilloud, N. Fray, Y. Benilan, H. Cottin, M.C. Gazeau and A. Jolly, MNRAS 451, 2145–2160 (2015)
42. A. G. G. M. Tielens, and S. B. Charnley, Origins Life Evol. B., 1997, **27**, 23
43. S. J. Blanksby, G. B. Ellison, *Accounts of Chemical Research*, 2003, **36**, 4, 255-263
44. N. Watanabe, A. Nagaoka, T. Shiraki, and A. Kouchi, The Astrophysical Journal, 2004, **616**, 638–642